1.B Numerical Modeling of Effects of Power Balance on Irradiation Nonuniformities

The need for good irradiation uniformity in inertial-confinement-fusion (ICF) target implosions has been well understood for some time.[1-6] In order to ignite and sustain thermonuclear burn, an ICF target must be symmetrically driven to very high densities [> 1000 times the liquid density of DT fuel (XLD)] while generating ignition temperatures (>5 keV).[7] The success of such implosion dynamics is dependent on the drive uniformity of the ablation front within the target. Perturbations at the ablation front are determined by the uniformity of the absorbed laser energy arriving from the critical surface. Although nonuniformities in this energy are smoothed in transit between the corona and the ablation surface,[1] the effect of any surviving nonuniformities is to perturb the hydrodynamic motion of the ablation front that can, in turn, serve to seed the possible secular and/or Rayleigh-Taylor unstable growth of this surface. Clearly, only very good irradiation uniformity can control these factors.

Laser irradiation nonuniformities can arise from several sources, including beam mispointing, energy and power imbalance, beam overlap due to the system geometry, and the individual profiles of the laser beams.[3] Over the past two years, it has become increasingly evident at LLE that improper power balance among the 24 OMEGA laser beams and poor laser-beam profiles have led to severe degradation of target performance when compared to one-dimensional predictions.[8] In attempting to model these nonuniformities it has been found useful to apply a spherical-harmonic decomposition of the applied radiation, since the effect on target performance is different for the long and short spatial wavelengths of nonuniformity.[6]

Calculations[3] (Table 41.I) have shown that power imbalance contributes to the long-wavelength structure ($\ell \lesssim 8$) while nonuniformities in the individual laser-beam profiles contribute primarily to the short-wavelength structure ($\ell \gtrsim 8$). Although there are mode-mode interactions between the two groups during an implosion, it is possible to evaluate the effects of each group separately. Significant effort has been exercised in analyzing and correcting the laser-beam profiles and is discussed in Refs. 9–13. This article will deal with evaluating the time-dependent sources of power imbalance that contribute to the long-wavelength perturbations.

The term "power balance" can be applied to a wide range of temporal, beam-to-beam intensity differences arising from laser amplifier saturation, variations in frequency conversion (detuning, polarization rotation, etc.), and/or the transport of energy from the conversion crystals to the target. Modeling the effects of these factors has required adapting our uniformity codes to treat time-dependent density and temperature profiles, as well as to include numerical models to simulate the individual power-imbalance contributions. Such an analysis will show that our efforts to control the tuning of the frequency-conversion crystals and the careful characterization of the UV transport losses have significantly reduced their contributions to

Table 41.I: Summary of the contributions of irradiation-nonuniformity sources to the various Legendre modes in ICF targets.

Modes	Source
$\ell = 1-4$	• pointing error • energy and power imbalance
$\ell = 8-12$	• beam overlap (24 –32 beams)
$\ell \gtrsim 8$	• beam imperfections

TC2780

the overall nonuniformity. However, effort still needs to be applied to characterize and correct misshaped pulses that can lead to very significant increases (factor of 3 to 5) in irradiation nonuniformity very early in the implosion.

We have divided this article into four sections: first, a discussion of the overall numerical method used to ascertain the nonuniformities; second, the individual contributions to power imbalance and illustrations of how they are modeled; third, numerical results showing how each of the power-imbalance terms affect the level of nonuniformity; and fourth, an experiment using the OMEGA laser system in which deliberate levels of power imbalance were applied. We also present a comparison of the experimental data with a simulation using the two-dimensional hydrodynamics code *ORCHID*.

Numerical Method

Several investigators have examined the uniformity produced by overlapping multiple laser beams on spherical targets.[1,3,14–17] Research at LLE has emphasized the decomposition of the laser energy in terms of spherical harmonics to obtain information about the spatial wavelengths of the nonuniformity on target for a given beam-overlap pattern.[3] The illumination pattern on target can be expressed as the product of two factors: (1) a "single-beam" factor that depends on the focal position, f-number of the lens, assumed target conditions, energy and possible temporal imbalance among individual beams (power balance), and the individual beam profiles; and (2) a "geometric" factor that is determined by the number and orientation of the individual beams about the target.

The method presented in this article is an adaptation of this previous work. It differs from that work in three main areas: First, instead of using an analytic, isothermal density profile, we use the one-dimensional hydrodynamics code *LILAC*[18] to provide time-dependent temperature and density profiles of the laser-absorption region. Second, our method considers the contribution of energy deposited between the critical surface and the surface determined by the position of the local peak in the electron temperature. The previous study considered only energy deposited between the critical and quarter-critical density surfaces. Finally, a full spherical-harmonic

decomposition of the absorbed energy is performed, allowing for the full phase information of the applied perturbation to be retained.

The actual calculation of the nonuniformity level starts by using *LILAC* to determine the temporal profiles of temperature and density, as opposed to previous treatments that assumed an analytical fit to the density profile under isothermal conditions. A two-dimensional geometrical optics ray-trace routine, taken from *ORCHID*, is employed to determine the azimuthally symmetric absorbed-energy profile due to a single beam. Several beam profiles, including patterns with time-dependent smoothing, can be considered. An angular source function is determined by collapsing (projecting) the absorbed energy to a single surface. This angular source function is then resolved into a series of Legendre polynomials.

Several prescriptions for collapsing the absorbed energy have been considered. Originally, only the energy between the critical and quarter-critical density surfaces (i.e., "quarter-critical cutoff") was considered to contribute to the intensity pattern.[3] However, since significant amounts of energy are deposited at densities less than quarter critical as an implosion proceeds, we believe that this cutoff is too restrictive and may have led to predictions of excessive nonuniformity levels. Other work[19] has shown that it is possible to weigh energy contributions from the entire corona as a function of density. However, the coefficients in such analytic formulations have to be recalculated several times during the implosion. Coefficients that yield good results early in the implosion become too optimistic at late times by allowing contributions from absorbed energy that cannot participate in the ablation process. A compromise has been found by examining the density and the electron-temperature profiles for a typical ICF implosion. It was found that there exists a maximum in the electron temperature outside of the quarter-critical density surface. Since thermal conduction is dominated by electron transport, it can be argued that only the energy at or within this temperature maximum will flow into the ablation region. Energy outside this region will flow out into the expanding corona and, as such, will not participate directly in determining the drive uniformity. Using the electron-temperature maximum cutoff, the absorbed energy between the critical surface and the cutoff is collapsed by radial integration to a single surface and a Legendre decomposition is applied to resolve the angular-source function into a single-beam series. A full mapping can then be made for the entire system of beams considered using this single-beam series.

The angle between each beam and a mapping location on the sphere is determined by the angle equation for two vectors on the unit sphere

$$\cos\gamma = \cos\theta\cos\theta' + \sin\theta\sin\theta'\cos(\varphi - \varphi'),$$

where θ and φ represent the coordinates of the laser beam and θ' and φ' are the coordinates of the mapping location. The single-beam series is evaluated for this angle to determine the intensity contribution of each laser beam to that location. The contribution of each beam can then be altered by a beam-balance factor due to the effects of power imbalance. How these factors are determined is discussed in the next section.

The procedure above is repeated for all beams over the sphere until a full spherical mapping is obtained. (Eventually we shall incorporate a full three-dimensional ray-trace routine to evaluate more realistic beam profiles. How such information might be incorporated into a two-dimensional hydrodynamics simulation is discussed later.) The mapping is now decomposed in spherical harmonics using a Laplace series involving the real functions $Y^e_{\ell m}$ and $Y^o_{\ell m}$,[20]

$$Y^e_{\ell m}(\hat{\Omega}) = P^m_\ell(\cos\theta)\cos m\varphi$$

$$Y^o_{\ell m}(\hat{\Omega}) = P^m_\ell(\cos\theta)\sin m\varphi$$

with

$$P^m_\ell(x) = \frac{1}{2^\ell \ell!}\left(1-x^2\right)^{m/2}\frac{d^{m+\ell}}{dx^{m+\ell}}\left(x^2-1\right)^\ell \qquad -\ell \le m \le \ell.$$

The intensity mapping $f(\hat{\Omega},t)$ can be expanded in these spherical harmonics as

$$f\left(\hat{\Omega},t\right) = \sum_{\ell}^{\infty}\sum_{m=0}^{\ell}\left[a_{\ell m}(t)Y^e_{\ell m}\left(\hat{\Omega}\right) + b_{\ell m}(t)Y^o_{\ell m}\left(\hat{\Omega}\right)\right]$$

where

$$a_{\ell m}(t) = \int d\hat{\Omega}\, f(\hat{\Omega},t)\, Y^e_{\ell m}(\hat{\Omega})$$

$$b_{\ell m}(t) = \int d\hat{\Omega}\, f(\hat{\Omega},t)\, Y^o_{\ell m}(\hat{\Omega})\ .$$

The traditional measure of the irradiation nonuniformity is the rms deviation defined as

$$\sigma_{\text{rms}}(t) = \left\{\frac{1}{4\pi}\int d\hat{\Omega}\left[f(\hat{\Omega},t) - f_0(t)\right]^2\right\}^{1/2}.$$

Performing the subtraction and employing orthogonality, this becomes

$$\sigma_{\text{rms}}(t) = \left\{\frac{1}{4\pi}\sum_{\ell=1}^{\infty}\sum_{m=0}^{\ell}\left[a^2_{\ell m}(t) + b^2_{\ell m}(t)\right]\right\}^{1/2}.$$

Since at present we do not have a three-dimensional hydrodynamics code available to simulate the full phase perturbations derived from such a decomposition, the phase information between the various modes is simply

summed together. This is accomplished by summing over the density of states

$$\alpha_\ell(t) = \sqrt{\frac{1}{4\pi}\sum_{m=0}^{\ell}\left[a_{\ell m}^2(t) + b_{\ell m}^2(t)\right]}.$$

The rms deviation of the nonuniformities is then given by

$$\sigma_{\text{rms}}(t) = \sqrt{\sum_{\ell=1}^{\infty}\alpha_\ell^2(t)}\ .$$

Since the growth of a particular ℓ-mode is degenerate with respect to all of its m-modes (i.e., the pure $m = 0$ harmonic grows the same regardless of its orientation on the sphere), the use of the α_ℓ terms works well when one is comparing the merits of one illumination scheme to another, or calculating the Rayleigh-Taylor growth of these modes throughout the implosion. However, one cannot use several α_ℓ terms directly in two-dimensional simulations because the phase orientations of the different azimuthally symmetric modes do not typically share the same vector on the unit sphere. (One could isolate a particular ℓ-mode on target through an appropriate choice of coordinates and have all of the $m \neq 0$ modes vanish. This would then represent a pure, azimuthally symmetric harmonic. It would then be possible to simulate the effects of this mode throughout the implosion using *ORCHID*. An experiment designed along these lines was performed and the results are presented later in this section.)

Modeling Power Imbalance

The effects of power imbalance are modeled by changing the deposition pattern of each beam by a beam-balance factor. While some sources of power imbalance are static, such as the reduced transmission in a turning mirror, most sources are time dependent and are related to beam misshaping and intensity mismatching. The beam-balance factor must therefore be calculated at each time step throughout the implosion. The modeling of each mechanism is now discussed.

Amplifier Saturation

Gain saturation in laser amplifiers results in changes to the shapes of individual pulses. We model these distorted pulses in two ways. The first method assumes all pulses are initially perfectly timed, equal-power Gaussians. Random analytic variations can then be applied to affect the arrival time, full width at half maximum (FWHM), and peak power of each of the individual pulses. This method, while not considering the effect of non-Gaussian pulse shapes, does provide the ability to consider a wide range of pulse distortions.

Recently, as described in article 1.A, it has become possible to evaluate some aspects of gain saturation, though it is still very difficult to determine experimentally the actual difference among all of the pulses, or the exact shape of an individual pulse.[21,22] However, it is now possible to determine a temporal power-ratio history between two of the separate infrared (IR) pulses. The power in each of the remaining beams is then assumed to lie in the envelope determined by this single beam-beam pair throughout the implosion. An important aspect of this method is that it does not restrict the

pulse shapes to be Gaussian. As these power histories become available for individual experiments, it will be possible to model each implosion with the correct amount of power imbalance due to gain saturation in the amplifiers.

Frequency-Conversion Crystal Detuning

The role of the frequency-conversion crystals in contributing to the total power imbalance in the laser system is due to their nonlinear response to the input laser intensity, as shown in Fig. 41.8. This response can vary significantly as a function of both the polarization angle of the input laser light and the amount of physical detuning of the tripler crystal from its optimum angle of 35° in relation to the "*e*" axis of the doubler crystal.[23] While the problem of controlling the polarization angle is easily solved by the introduction of a polarizer just in front of the conversion crystals, errors in tuning the crystals can be corrected by only a small amount. Typically, manual settings can routinely yield variations of about 100 μrad among our 24 beams. However, as discussed below, this amount of detuning does not contribute considerably to the overall nonuniformity present in our implosions.

The real impact of the conversion crystals on power imbalance comes when one considers the effects of their nonlinear response to input pulses with varying intensities. It can be seen in Fig. 41.8 that very significant perturbations in beam power can result due to the variance in conversion efficiency at the different input intensities. Any intensity variations among pulse shapes, such as those discussed in the previous section, can be significantly enhanced by the conversion process.

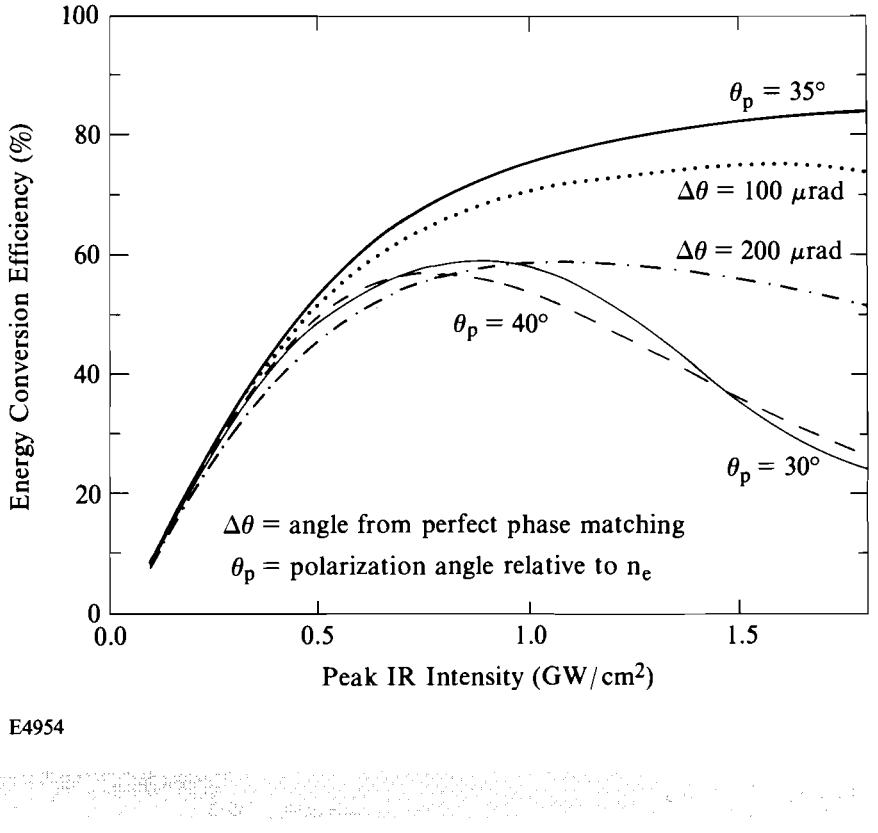

Fig. 41.8
Third-harmonic energy-conversion efficiency for type II - type II tripling in two 16-mm-thick KDP crystals for various tuning conditions.

To model the response of the conversion crystals, polynomial fits of the conversion efficiency as a function of the input intensity were obtained.[24] Such fits were provided for cases of optimal and 100-μrad detuning. At the beginning of each simulation, the crystal in each beamline was given a random detuning between optimal and 100 μrad that was fixed throughout the implosion. At each time step during the simulation, the input intensity into each crystal was calculated and an interpolation between the two fits provided the appropriately degraded conversion efficiency. These numbers were then factored into calculating the overall beam-balance factor used in distributing the energy over the sphere.

Transport Losses

The last effect to be modeled is transmission losses due to the system of transport optics that delivers the UV-converted light from the conversion crystals to the target. This system consists of turning mirrors, distributed phase plates (DPP's), focusing lenses, and blast windows. Any defects in these elements can affect the overall transport efficiency to the target. While the transmission characteristics of these elements can be tested to very high accuracy when removed from the OMEGA system, it has been very difficult to measure them while deployed on the system. Recently, however, a new system has been activated that can measure the transmission characteristics to within ±0.3%.[25] The OMEGA transport-integrating sphere (OTIS) can now routinely measure the transport on a weekly basis and has shown that variations in the transport efficiencies are in the range of ~5% peak-to-valley.

Using the information from the OTIS measurements, a simple fraction can be factored into the beam-balance factor. This number represents a static power imbalance throughout the pulse. As will be shown in the next section, variations in the transport losses in the range of 5% do not contribute significantly to the overall nonuniformities placed on target.

Numerical Evaluation of Power Imbalance

Using the numerical models described above, it is now possible to evaluate the effects of the various contributions on the level of nonuniformity. To provide a good approximation to our current experiments, the input power of each of the individual pulses is tuned to reflect the experimentally recorded, time-integrated energy balance. (Typically, the overall energy balance is in the range of 10% peak-to-valley.) We have chosen to use a laser-beam profile, shown in Fig. 41.9, that produces a level of nonuniformity characteristic of beams smoothed by spectral dispersion (SSD). This laser profile was constructed using a modified Airy pattern[9] of the form

$$I(\bar{r}) = g(\bar{r})\left[\frac{2J_1(\pi\bar{r})}{\pi\bar{r}}\right]^2,$$

where

$$\bar{r} = \left(r / r_o\right)_{\text{beam}} .$$

The function $g(\bar{r})$ includes the effects of small scale variations of the radial beam shape due to diffraction rings,[3] and is defined as

$$g(\bar{r}) = [1 + \epsilon \cos(\pi N \bar{r})].$$

Modulation parameters of $N = 3$ and $\epsilon = 0.1$ are used here.

We considered a typical OMEGA glass-ablator target that is shown schematically in Fig. 41.10. The pellet consists of a 5-μm-thick glass shell with an inner diameter of 240 μm and filled with 25 atm of deuterium. The target has been overcoated with 500 Å of aluminum to prevent any early shine-through effects.[26] *LILAC* was used to provide the time-dependent temperature and density profiles for this particular target when imploded by a 1300-J, 351-nm, 620-ps (FWHM) pulse. The nonuniformities due to four different scenarios were then calculated and the results appear in Fig. 41.11.

The first scenario simulated was the case of perfect power balance throughout the system. This result is shown as curve A in Fig. 41.11. One can see that initially the total nonuniformity is ~4% σ_{rms} and is in good agreement with other calculations done for the asymptotically smoothed SSD beam. To determine the source of this nonuniformity, it is possible to view the contributions for the individual ℓ-modes. Figures 41.12 and 41.13 show the distribution of the various ℓ-modes for each of the four scenarios at two times during the implosion (marked 1 and 2 in Fig. 41.11). Evaluating the particular modes for curve A, it can be seen that the nonuniformity is due solely to those modes that are affected by the beam-placement geometry of 24 beams (i.e., $\ell = 4$, 8, and 10).[3]

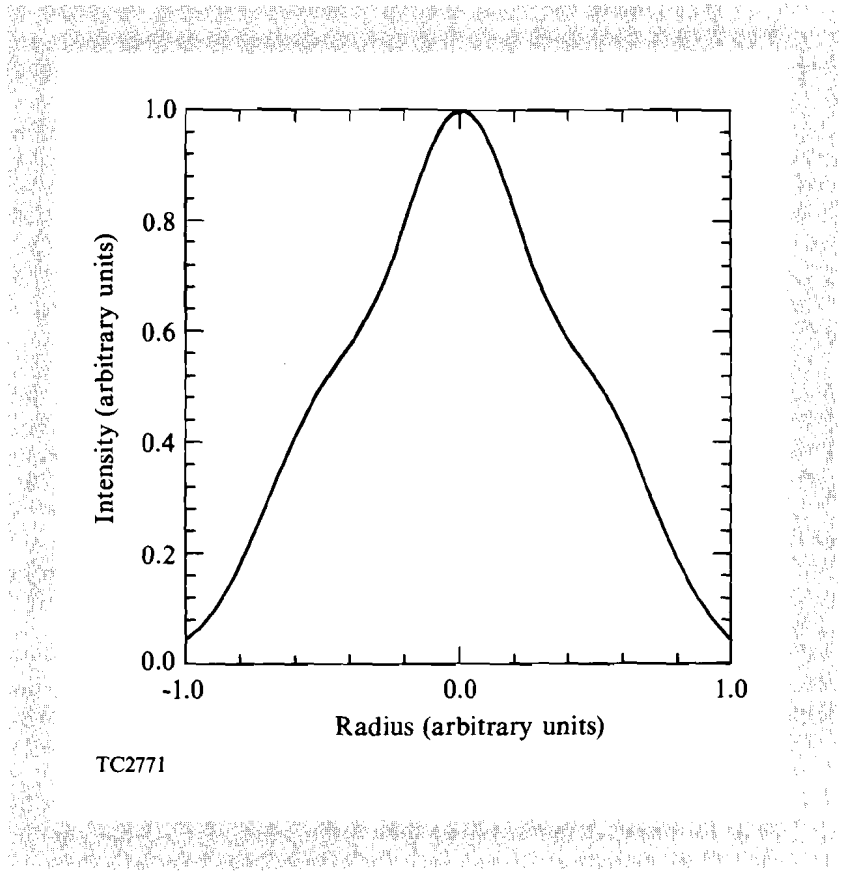

Fig. 41.9
Asymptotically smoothed, SSD laser-beam profile used in the calculations.

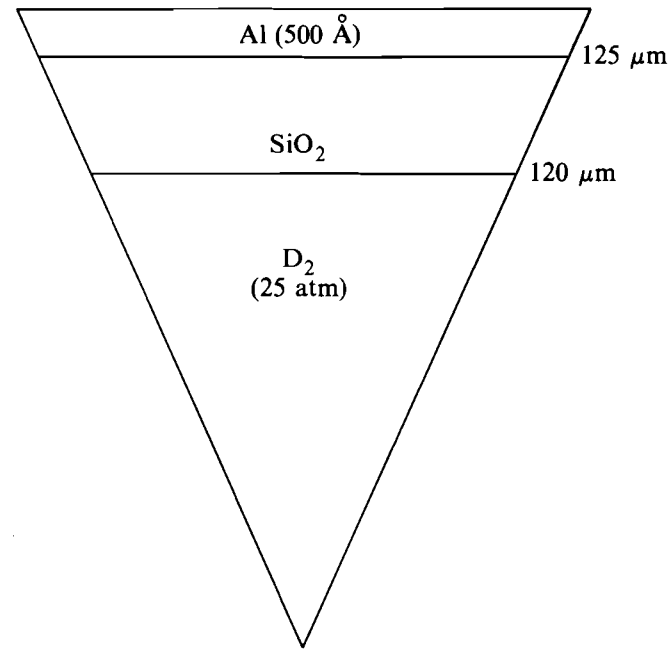

Fig. 41.10
Schematic of a single-shell, glass-ablator, OMEGA high-density pellet.

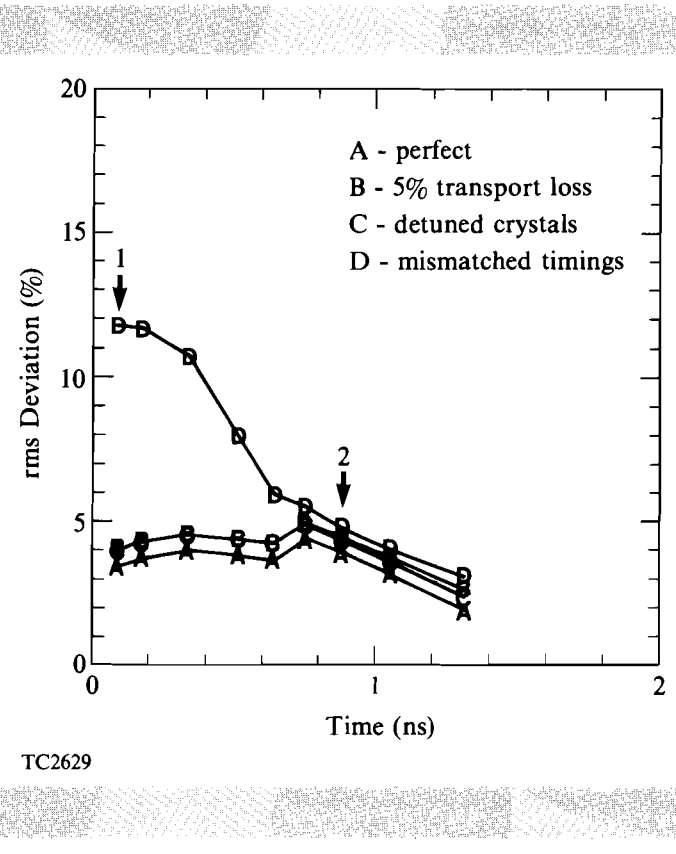

Fig. 41.11
Calculated rms deviation for four different illumination scenarios.
(A) Perfect power balance throughout the laser system.
(B) 5% peak-to-valley random variations in the transport optics in each of the 24 OMEGA beamlines.
(C) In addition to B, a random detuning in each of the 24 frequency-conversion crystals from 0 to 100 μrad.
(D) Including B and C, a 5% random variation in both beam-arrival time and FWHM.

The ℓ-mode spectra at times 1 (30 ps) and 2 (900 ps) in the implosion are given in Figs. 41.12 and 41.13, respectively.

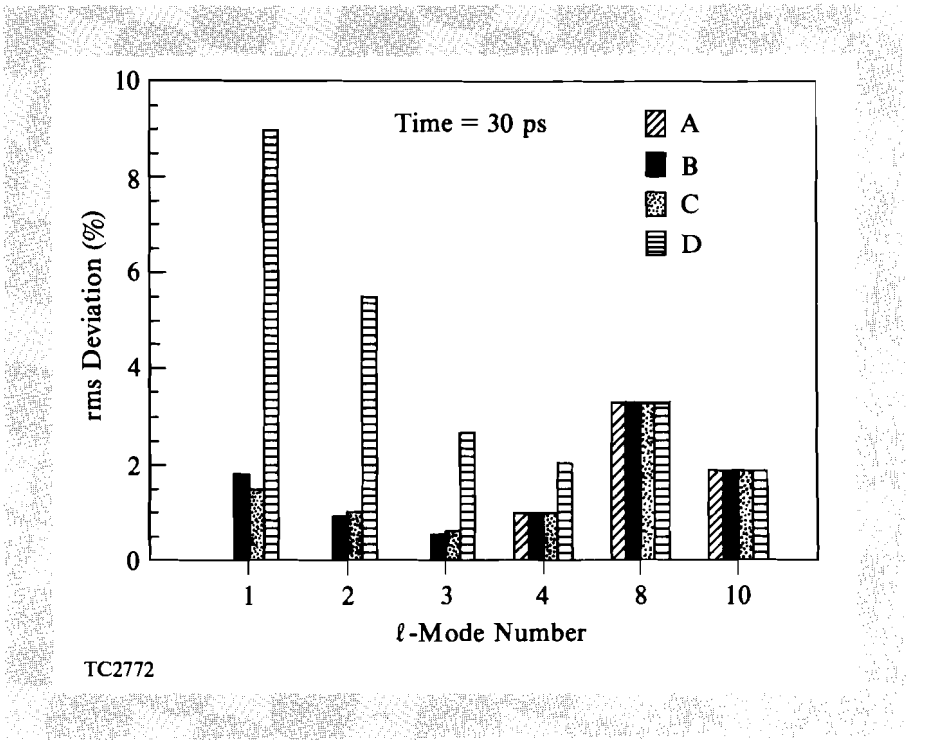

Fig. 41.12
Legendre ℓ-mode spectrum evaluated at 30 ps into the implosion. (This corresponds to point 1 in Fig. 41.11).

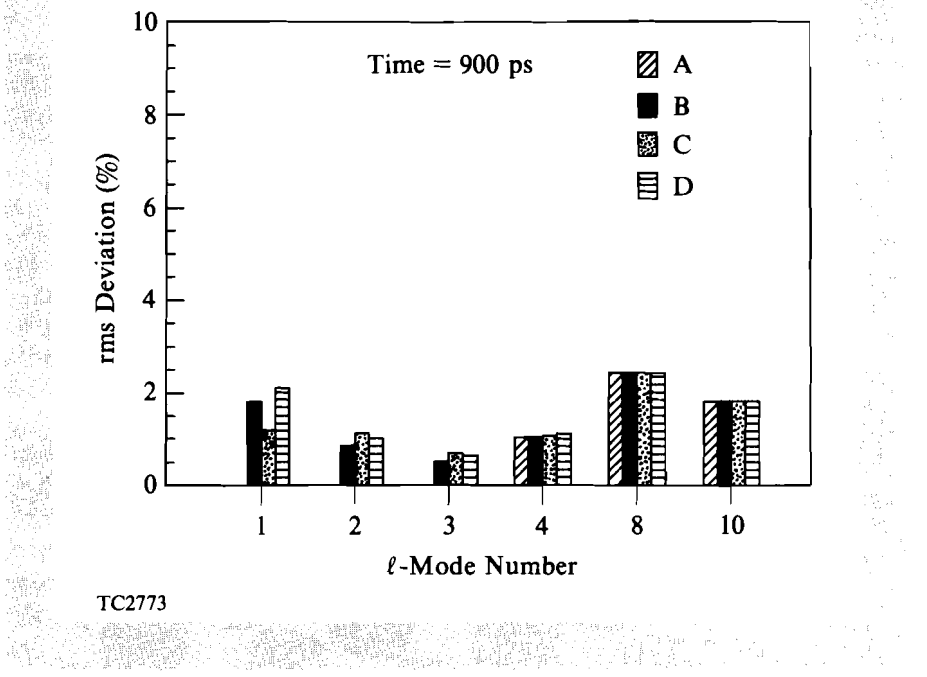

Fig. 41.13
Legendre ℓ-mode spectrum evaluated at 900 ps into the implosion. (This corresponds to point 2 in Fig. 41.11).

The second scenario assumed that the transport losses between the frequency-conversion crystals and the target have a random 5% peak-to-valley variation among all beams. From curve B in Fig. 41.11 we see a modest increase in the applied nonuniformity as a function of time. Examining the ℓ-mode distribution, it can be seen that there are now contributions from the $\ell = 1, 2$, and 3 modes. These contributions are almost constant throughout the implosion, as can be seen from Fig. 41.13.

The next scenario considered the application of a random detuning from 0 to 100 μrad to each of the 24 conversion crystals in addition to the 5% transport variations of the second scenario. The results of this third scenario are shown as curve C in Fig. 41.11. The fact that there is very little difference between the second and third scenarios illustrates how the various contributions to nonuniformity add in quadrature, so that even though the applied spectrum can differ, the overall effect can remain unchanged or, in some cases, actually improve.

In the last scenario we attempt to fully model all of the factors contributing to power imbalance on OMEGA. In addition to the factors of the third scenario, the arrival times and shapes of all 24 laser pulses are each randomly varied by 5% peak-to-valley. Such pulse variations lead to a much higher total nonuniformity level early in the implosion as can be seen from curve D in Fig. 41.11. All modes from $\ell = 1$ to 4 are significantly excited early in the implosion. However, as the implosion proceeds, the power balance among the individual beams improves and we recover the results of the second and third scenarios. This can also be seen in Fig. 41.13 where the highly excited low-order modes seen in Fig. 41.12 have calmed down significantly.

Reviewing the results of the four separate scenarios, it can be seen that our efforts to characterize and correct problems with transport losses and conversion-crystal detuning have resulted in these factors making only a small contribution to the overall level of nonuniformity on target. However, as the fourth scenario illustrates, problems with pulse shapes and timing can lead to very large pertubations at early times in our implosions.

Power-Imbalance Experiment

Experimental verification of the calculated nonuniformity levels within ICF targets is a major goal of the LLE direct-drive program. However, there have been few, if any, experimental diagnostics available with the spatial and temporal resolution required to provide useful information about the existence of the predicted nonuniformities. Recently, however, with the advent of the x-ray-framing cameras developed at the Lawrence Livermore National Laboratory (LLNL),[27] it has become possible to diagnose relatively long duration ($\gtrsim$ 50-ps), large (>10-μm) perturbations during the implosion. The serpentine x-ray-framing camera,[28, 29] shown schematically in Fig. 41.14, allows for 14 x-ray images, separated by ~47 ps, during the implosion. The spatial resolution is determined by the individual size of each pinhole in the pinhole array. (For our camera this is typically 12 μm.) The deployment of this diagnostic on OMEGA has enabled the characterization of an experiment in which a deliberate power imbalance was applied. The level of nonuniformity present in the experiment was calculated and then used in a two-dimensional *ORCHID* simulation. The correlation of experiment and simulation tends to validate our estimates of the nonuniformity present.

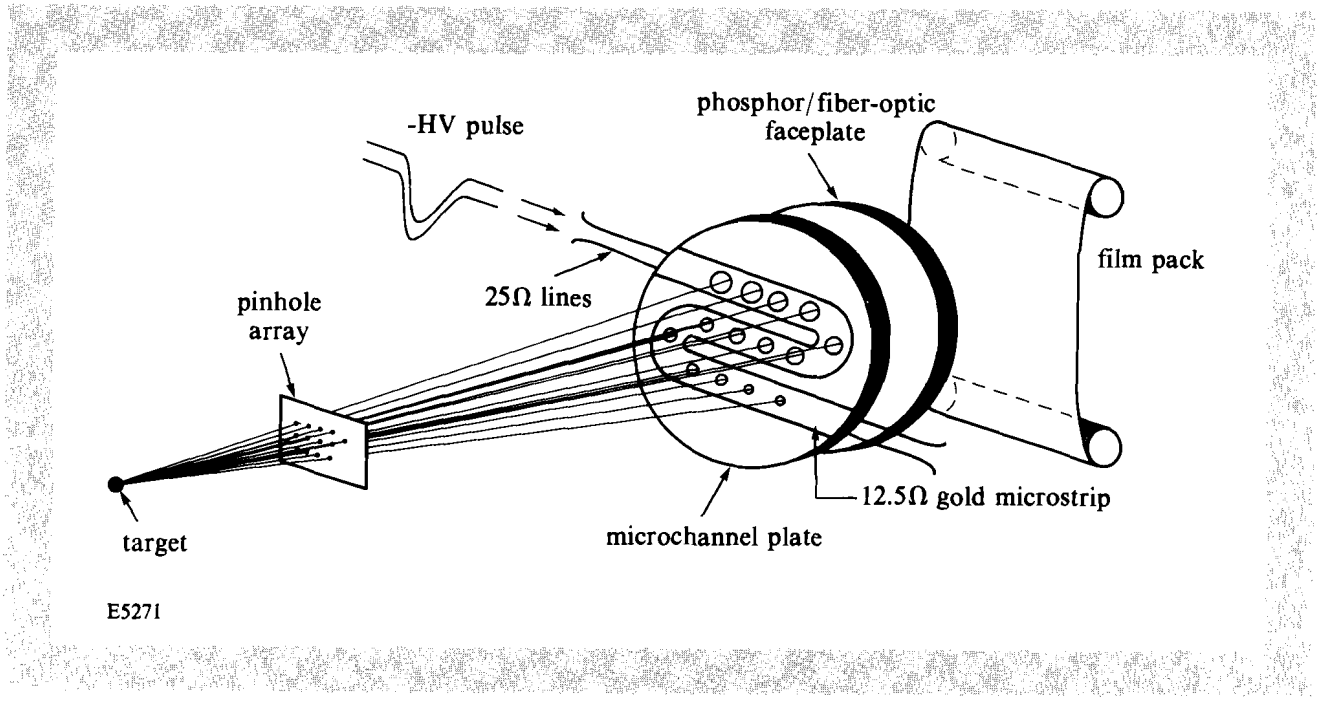

Fig. 41.14
Schematic of the serpentine x-ray-framing camera deployed on the OMEGA laser system.

The design of a power-imbalance experiment presented two challenges. The first involved manipulating the laser beams such that a particular mode would be imprinted on the target with sufficient strength to both dominate all other modes present and be detectable by the diagnostic. The second challenge was based on our desire to use *ORCHID* to simulate the implosion. Because *ORCHID* assumes azimuthal symmetry, it was necessary to isolate the pure $m = 0$ component of the imprinted ℓ-mode.

The mode we chose to imprint was the $\ell = 1$ mode. This was accomplished by employing beam clusters 2 and 5 on the OMEGA laser system. The energy of these beams was increased (cluster 2) or decreased (cluster 5) by ~20% from the mean. It was estimated that a ~ 40% peak-to-valley, $\ell = 1$ mode should then result on target. The decomposition of this illumination pattern, given in Fig. 41.15, confirmed the large $\ell = 1$ contribution imprinted on target. Analysis of the phase information identified several ports on the OMEGA target chamber, including port #133, whose lines of sight were almost directly perpendicular to the plane formed between clusters 2 and 5. Using the orientation of port #133, 96% of the $\ell = 1$ mode exists in the $m = 0$ harmonic (i.e., almost purely azimuthally symmetric). The serpentine camera was positioned in port #133 such that the applied illumination pattern would be recorded with the maximum intensity of cluster 2 on the left-hand edge of the film plane.

The data from this experiment are shown in Fig. 41.16. As the implosion proceeds (the frames follow a reversed "*S*" configuration with time), it can be seen that the imploded core is in fact pushed off center by the applied

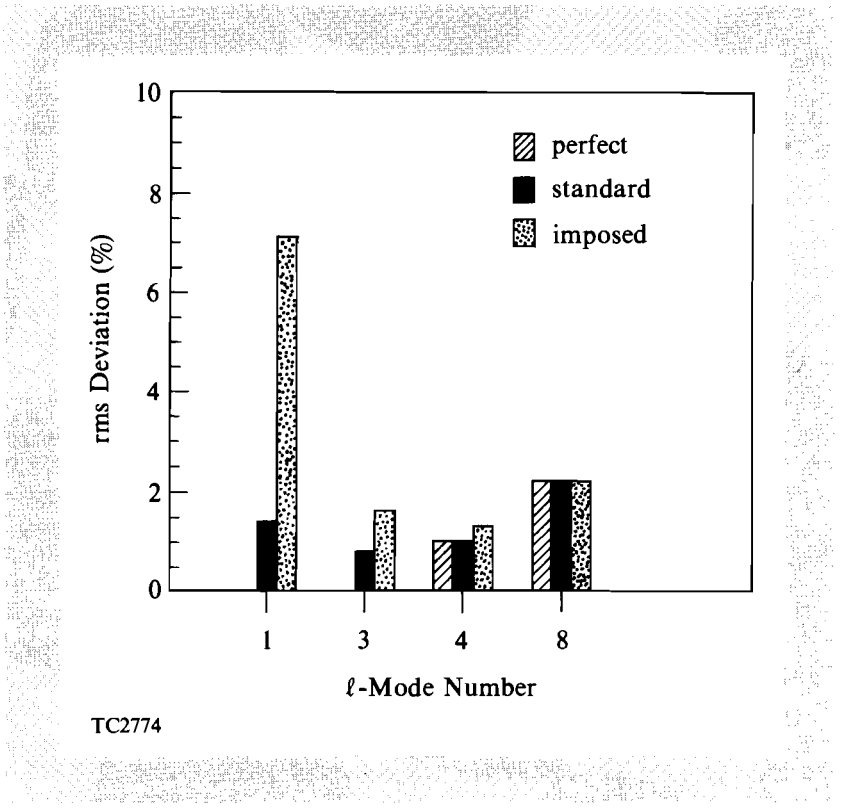

Fig. 41.15
Comparison of the calculated ℓ-mode spectra for perfect power balance, typical OMEGA power imbalance, and the imposed power-imbalance experiment.

perturbation. In Fig. 41.17 we have selected an individual frame for analysis that is approximately 300 ps after the peak of the pulse. The geometric center of the limb emission for this frame was determined and an azimuthal average gives the intensity as a function of the radial position as shown in Fig. 41.18. From Fig. 41.18, it can be seen that the core has formed approximately 6 μm to 10 μm to the right of center during the implosion. The limbs appear almost circular and are located at ~ ±45 μm from the center.

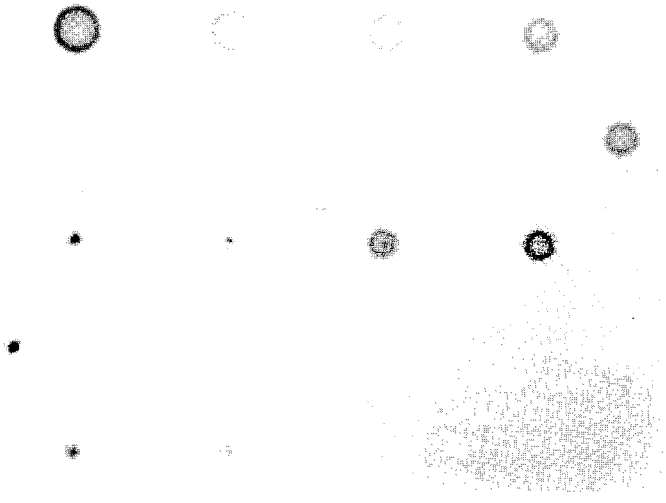

Fig. 41.16
Experimental data obtained using the serpentine x-ray-framing camera for OMEGA shot #18682. The initial target diameter was 250 μm. The individual frames are separated by ~47 ps and are "open" for ~100 ps.

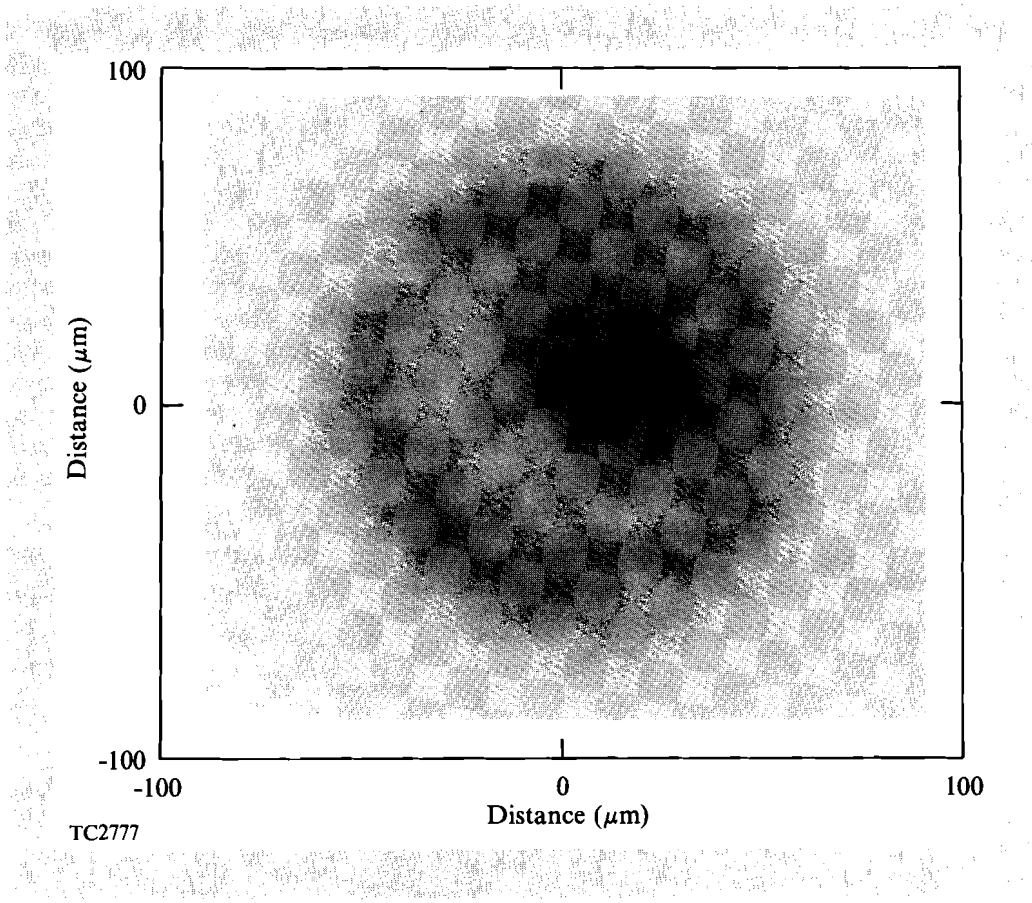

Fig. 41.17
Individual x-ray-framing image taken from Fig. 41.16 (frame H). This particular frame was approximately 300 ps after the peak of the pulse.

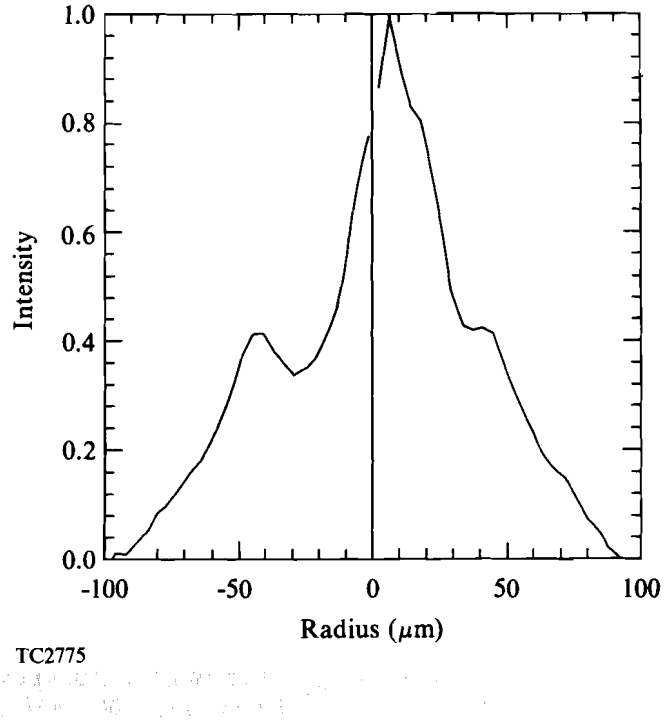

Fig. 41.18
Azimuthally averaged intensity profiles over both left- and right-hand sides of image shown in Fig. 41.17. An average about the geometric center of the limb emission is used to obtain each profile.

The time-dependent nonuniformity calculated for this implosion was then used as input to an *ORCHID* simulation. Only the dominant modes ($\ell = 1, 2, 3$, and 8) were simulated. The implosion was simulated to a time that was comparable to the frame chosen and the results are presented in Fig. 41.19. From the grid plot [Fig. 41.19(a)], the simulation prediction for the position of the imploded core is close to that observed in the experiment. Determination of the limb-emission location requires evaluating a contour plot of the electron temperature. The limb emission should peak in the region between 800 eV to 1000 eV. The electron-temperature isotherms are plotted in Fig. 41.19(b) and the position of the 800-eV isotherm, relative to the center of the implosion, is again in good agreement with the experimental data. This correlation between the experiment and simulation is very encouraging. We hope to repeat a more extensive set of these experiments, evaluating not only other ℓ-modes, but also examining how the overall target performance (i.e., neutron yield) is affected by the presence of various applied nonuniformities.

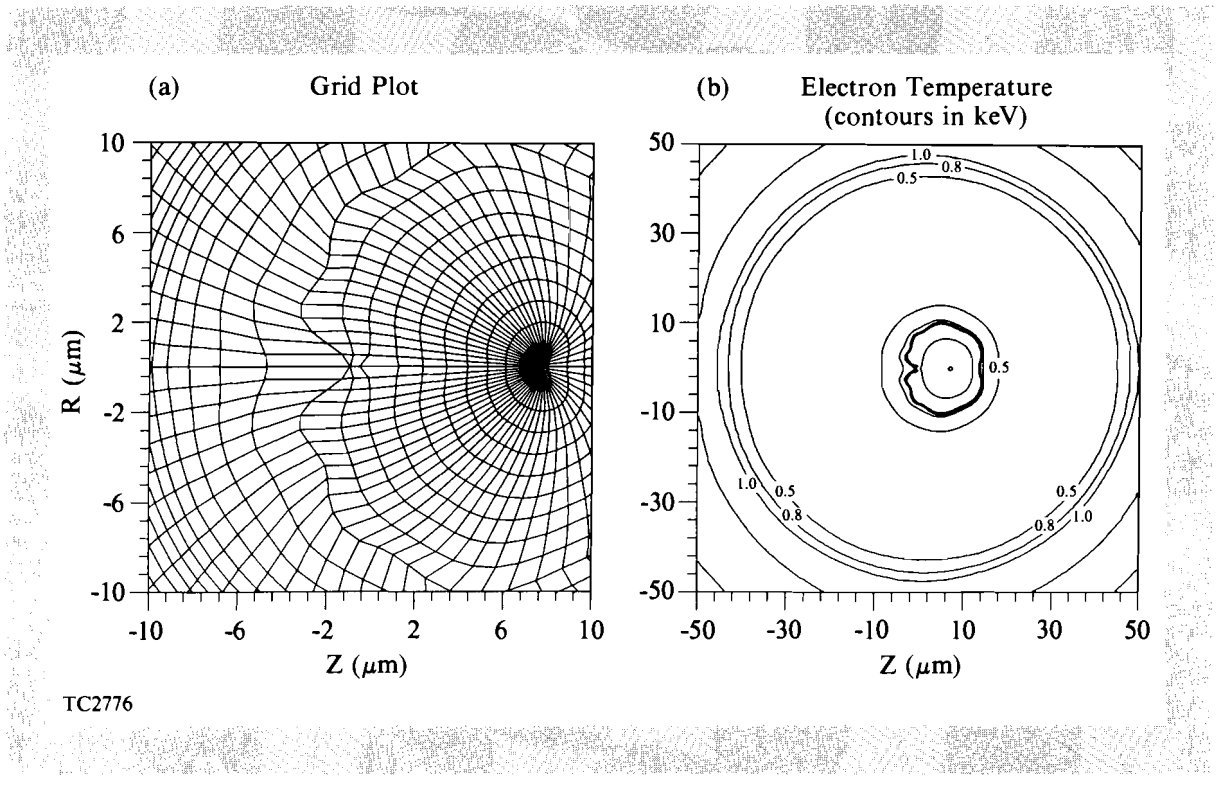

Fig. 41.19
Two-dimensional (*ORCHID*) hydrodynamics simulation of the single-shell OMEGA target shown in Fig. 41.11.

(a) The grid plot has been expanded to display the position of the imploded core at 1290 ps into the implosion. The core has formed ~7 μm to the right of center.

(b) Contour map of the electron temperature at 1290 ps into the implosion. The limb emission (~800 eV to 1000 eV) is predicted to be circular with a radius of ~45 μm.

Conclusion

Power imbalance among the 24 OMEGA laser beams can produce significant long-wavelength irradiation nonuniformities on target during implosions. We have adapted our uniformity codes to incorporate time-

dependent density and temperature profiles obtained from *LILAC* simulations of the experiments. The various sources of power imbalance on the OMEGA system have been characterized and modeled numerically. From the analysis it has been shown that the levels of power imbalance due to frequency-conversion crystal detuning and UV-transport losses, when managed properly, make only a modest contribution to the overall nonuniformity. However, this analysis also shows that significant nonuniformity can be imprinted on the target early in the implosion due to pulse misshaping. Finally, an experiment involving deliberately applied levels of power imbalance was undertaken and then simulated with *ORCHID* using estimates of the applied perturbation. Good correlation was found between the experimentally observed core positions and those predicted by the *ORCHID* simulation. Further experimental investigations are in progress.

ACKNOWLEDGMENT

This work was supported by the U.S. Department of Energy Division of Inertial Fusion under agreement No. DE-FC03-85DP40200 and by the Laser Fusion Feasibility Project at the Laboratory for Laser Energetics, which has the following sponsors: Empire State Electric Energy Research Corporation, New York State Energy Research and Development Authority, Ontario Hydro, and the University of Rochester.

REFERENCES

1. S. E. Bodner, *J. Fusion Energy* **1**, 221 (1981).
2. J. H. Nuckolls, *Phys. Today* **35**, 24 (1982).
3. S. Skupsky and K. Lee, *J. Appl. Phys.* **54**, 3662 (1983).
4. S. Skupsky, R. L. McCrory, R. S. Craxton, J. Delettrez, R. Epstein, K. Lee, and C. P. Verdon, *Laser Interaction and Related Plasma Phenomena*, edited by H. Hora and G. H. Miley (Plenum, New York, 1984), Vol. 6, p. 751.
5. LLE Review **23**, 125 (1985).
6. LLE Review **37**, 1 (1988).
7. J. Nuckolls, L. Wood, A. Thiessen, and G. Zimmerman, *Nature* **239**, 139 (1972).
8. LLE Review **37**, 1 (1988).
9. LLE Review **33**, 1 (1987).
10. LLE Review **37**, 29 (1888).
11. LLE Review **37**, 40 (1988).
12. S. Skupsky and T. Kessler, *Opt. Commun.* **70**, 123 (1989).
13. S. Skupsky, R. W. Short, T. Kessler, R. S. Craxton, S. Letzring, and J. M. Soures, *J. Appl. Phys.* **66**, 3456 (1989).
14. *Laser Program Annual Report, 1974*, #UCRL-50021-74, edited by J. I. Davis and W. Clements [(California University, Lawrence Livermore Laboratory, Livermore (USA), 1975)], p. 519.
15. J. E. Howard, *Appl. Opt.* **16**, 2764 (1977).
16. A. J. Scannapieco and H. Brysk, *J. Appl. Phys.* **50**, 5142 (1979).
17. LLE Lab Report No. 88 (1981).

18. LLE Lab Report No. 16 (1973).

19. A. J. Schmitt and J. H. Gardner, *J. Appl. Phys.* **60**, 6 (1986).

20. G. B. Arfken, *Mathematical Methods for Physicists*, 3rd ed. (Academic Press, New York, 1985), p. 683.

21. P. A. Jaanimagi, J. Kelly, R. Keck, W. Seka, and R. Saunders, *Bull. Am. Phys. Soc.* **34**, 2041 (1989).

22. R. L. Keck, J. P. Knauer, S. Letzring, S. Morse, W. D. Seka, and J. M. Soures, *Bull. Am. Phys. Soc.* **34**, 2041 (1989).

23. R. S. Craxton, *Opt. Commun.* **34**, 474 (1980).

24. R. S. Craxton and J. P. Knauer (private communication).

25. LLE Review **38**, 111 (1989).

26. LLE Review **35**, 125 (1988).

27. J. D. Kilkenny *et al.*, *Rev. Sci. Instrum.* **59**, 1793 (1988).

28. D. K. Bradley, J. Delettrez, P. A. Jaanimagi, C. P. Verdon, J. D. Kilkenny, and P. Bell, *Bull. Am. Phys. Soc.* **34**, 1962 (1989).

29. P. E. Bell, J. D. Kilkenny, G. Power, R. Bonner, and D. K. Bradley, *Ultra High Speed Photography, Videography, and Photonics VII* (SPIE, Bellingham, WA, 1989), to be published.